Ultrasonics Sonochemistry 19 (2012) 1252–1259

Contents lists available at SciVerse ScienceDirect

Ultrasonics Sonochemistry

journal homepage: www.elsevier.com/locate/ultson

Sonoluminescence and sonochemiluminescence from a microreactor

David Fernandez Rivas [a,*], Muthupandian Ashokkumar [b], Thomas Leong [b], Kyuichi Yasui [d], Toru Tuziuti [d], Sandra Kentish [b], Detlef Lohse [c], Han J.G.E. Gardeniers [a]

[a] Mesoscale Chemical Systems, MESA + Research Institute, University of Twente, ME147, P.O. Box 217, 7500AE Enschede, The Netherlands
[b] School of Chemistry, Department of Chemical and Biomolecular Engineering, University of Melbourne, VIC 3010, Australia
[c] Physics of Fluids Group, Department of Applied Physics, Faculty of Science, University of Twente, P.O. Box 217, 7500AE Enschede, The Netherlands
[d] National Institute of Advanced Industrial Science and Technology (AIST), Moriyama ku, Nagoya 463 8560, Japan

ARTICLE INFO

Article history:
Received 10 January 2012
Received in revised form 10 April 2012
Accepted 14 April 2012
Available online 3 May 2012

Keywords:
Sonochemistry
Ultrasound
Sonoluminescence
Sonochemiluminescence
Microbubbles
Microreactors

ABSTRACT

Micromachined pits on a substrate can be used to nucleate and stabilize microbubbles in a liquid exposed to an ultrasonic field. Under suitable conditions, the collapse of these bubbles can result in light emission (sonoluminescence, SL). Hydroxyl radicals (OH·) generated during bubble collapse can react with luminol to produce light (sonochemiluminescence, SCL). SL and SCL intensities were recorded for several regimes related to the pressure amplitude (low and high acoustic power levels) at a given ultrasonic frequency (200 kHz) for pure water, and aqueous luminol and propanol solutions. Various arrangements of pits were studied, with the number of pits ranging from no pits (comparable to a classic ultrasound reactor), to three-pits. Where there was more than one pit present, in the high pressure regime the ejected microbubbles combined into linear (two-pits) or triangular (three-pits) bubble clouds (streamers). In all situations where a pit was present on the substrate, the SL was intensified and increased with the number of pits at both low and high power levels. For imaging SL emitting regions, Argon (Ar) saturated water was used under similar conditions. SL emission from aqueous propanol solution (50 mM) provided evidence of transient bubble cavitation. Solutions containing 0.1 mM luminol were also used to demonstrate the radical production by attaining the SCL emission regions.

1. Introduction

A well known effect of ultrasonic irradiation in a liquid is acoustic cavitation, which is the nucleation and consequent collapse of bubbles [1]. Sometimes, bubbles can cavitate in phase with the applied sound frequency. These bubbles behave as "individual microreactors", as they are often accompanied by a violent collapse that leads to high pressures and temperatures within and in the local vicinity of the bubbles [2–4]. Among the events generated during such collapses, some can be identified as plasma formation, lysis of molecules yielding radicals (water molecule sonolysis is a well known example), strong pressure shockwaves, liquid jetting and surface erosion. Although the driving condition is constant in most cases, the cavitation bubbles are never exactly the same due to the complexity of the phenomena involved [5], rendering it difficult to obtain a deterministic relation between driving conditions and actual bubble population. To complement direct determination of bubble size distributions which require fast imaging and intensive image processing, a good alternative is the use of indirect methods like measuring the light emitted by these bubbles.

Most researchers agree that the studies of Marinesco and Trillat [6] and Frenzel and Shultes [7] were the first in which light emission could be detected as a result of ultrasound irradiation in a liquid sample. After several studies to determine the actual mechanism behind this remarkable effect, sonoluminescence (SL) has been described as the light emitted by cavitation bubbles driven by an ultrasonic driving pressure field. Sonochemiluminescence (SCL) is defined in this study as the light emission when luminol reacts with OH· radicals. There is a large difference between the SL emission from a single bubble (SBSL) and SL from a cluster of bubbles (MBSL, i.e., multibubble SL). For SBSL the collapse is nearly spherically symmetric and highly reproducible [4]; and for MBSL the more frequent non repeatable asymmetric collapse produces liquid jets penetrating the hot bubble contents [8–11]. These differences are evident in the emission profile and spectra produced from both types of SL. The spectra collected from MBSL contain many peaks and features, whereas the spectra emanating from SBSL are normally featureless [12,13]. The effect of power and frequency on bubble-size distributions of MBSL in acoustic cavitation has been studied previously using pulsed ultrasound [14]. The main conclusion was that the mean bubble size increased with increasing acoustic power and at the same time decreased with increasing ultrasound frequency. Additionally, the

* Corresponding author. Tel.: +31 534892594.
E-mail address: d.fernandezrivas@utwente.nl (D. Fernandez Rivas).

1350-4177/$ - see front matter © 2012 Elsevier B.V. All rights reserved.
http://dx.doi.org/10.1016/j.ultsonch.2012.04.008

mean bubble size distribution of bubbles emitting SL was larger and narrower than SCL producing bubbles (centred at smaller bubble sizes and broader) meaning that the two processes result from different bubble sizes [15] and the physical locations in which these bubbles exist can differ [16]. MBSL has also a defined phase window of the driving pressure oscillation, meaning that in a phase window of about 30° from the full 360° SL can be detected [5]. Other researchers have reported singular dependences of SL and capillary pressure in small gaps with an implicit advantage in not using a light-proof box to quantify multibubble intertial cavitation thresholds [17].

Sonochemistry performed in microfluidic devices has received some attention in the last decade [18–21]. In this work, an extended study on an ultrasonic microreactor described before [18] is presented. The working principle of that sonoreactor is based on the ability of small predefined crevices (pits etched in silicon substrate surface [22–25]) to stabilize small gas nuclei. When the ultrasound is turned on, a characteristic microbubble cloud appears, that would not be present in the absence of pits. In this way a continuous locally controlled generation of cavitating microbubbles is achieved. The chemical activity of these microbubbles was previously verified by luminol SCL imaging and $OH^{\cdot}$ radical dosimetry by using terephthalic acid [18].

The aim of the present work was to study the changes of SL and SCL intensities emanating from different solutions as the population of microbubbles nucleated from the pits on the silicon substrate varies. This is influenced by altering the power input to the system and the number of pits. The areas of potential application for these findings are many; to name a few we consider the ultrapurification of water for fine chemicals or pharmaceutical uses, mechanochemistry and the selective cleaning of circuit boards in which localized cavitation can avoid the damage of certain components with conventional sonication systems [26,27]. Our results can be of importance to existing non destructive testing and inspection of surfaces with localized fluorescent dye penetration which are improved by the action of localized cavitation [28].

Additionally for biological applications where a localized source of radicals, light and streaming forces are required, this system might be beneficial [29,30].

2. Material and methods

This work focused on the measurement of the SL and SCL intensities emitted from three different systems. The first was air-saturated Milli-Q water, the second was air saturated propanol solution (50 mM) in water and the third was air saturated aqueous luminol (0.1 mM luminol in 0.1 M NaOH) solution. SL intensities were obtained for water and propanol, whereas SCL intensities were measured for luminol. Additionally SL images were recorded in argon saturated water.

In most cavitating systems, there exist populations of SL active and SCL active bubbles [31]. These populations strongly overlap: SL active bubbles can be SCL active, and vice versa. SL active bubbles correspond to bubbles that satisfy suitable conditions (pressure and temperature) inside the bubble that allow for ionization and the subsequent light emission [32]. SCL active bubbles produce radicals ($OH^{\cdot}$ radicals in this case):

$$H_2O \rightleftharpoons OH^{\cdot} + H^{\cdot} \quad (1)$$

Recording the light emission from luminol molecules reacting with $OH^{\cdot}$ is a widely used method to quantify the chemical activity and map active zones in a sonoreactor. Evidently knowing the exact bubble size distribution and their spatial localization is very difficult ([33–35]), and most studies are based on bubble dissolution when US is turned off [14,36,37]. By virtue of dissolved propanol in water, information about the presence of transient cavitating bubbles can be obtained [38,39]. It has been shown that alcohols do not quench SL arising from transient cavitation (i.e., MBSL), as the alcohol molecules do not have enough time to accumulate on the interface of the transiently cavitating bubbles [39]. That is in vast contrast to stable SBSL, where alcohols strongly quench the light emission [40].

2.1. Set-up for US experiments

A scheme of the experimental setup used is shown in Fig. 1. The reaction chamber was a glass container of 25 mm outer diameter, 15 mm inner diameter and depth of 2 mm, and bottom thickness of 2 mm. The bottom thickness matched the quarter-wavelength vibration imparted by a piezo Ferroperm PZ27 6 mm thick with a diameter of 25 mm, glued to the bottom of the reaction chamber.

The ultrasonic wave was generated by a Hameg HM 8131-2 arbitrary waveform generator and amplified by a Krohn–Hite Model 7500 amplifier for the sonochemical reaction experiments and a LeCroy WaveSurfer 452 oscilloscope to read-out PMT measurements.

The powers used for the experiments were calculated from calorimetric measurements with a Hanna K-type Thermocouple leading to 12.7 W for the high power and 3.32 W for the low power settings. Since control over the heating of the liquid volume was not available, temperature measurements were carried out before and after irradiation times of 3 min at similar conditions at which the SL and SCL signals were recorded. The thermocouple was removed from the liquid chamber during sonication to avoid damaging the thermocouple tip. At low power (3.32 W) the temperature did not increase by more than 3 K. For high power (12.7 W) the temperature increase was of 10 K. The 10 s period would generate an increase in temperature of around 0.6 K. We overestimate the temperature increase to be at least 1 K (2 K maximum) to be conservative. For this reason, the PMT measurements lasted in general no longer than 10 s to avoid large temperature variations.

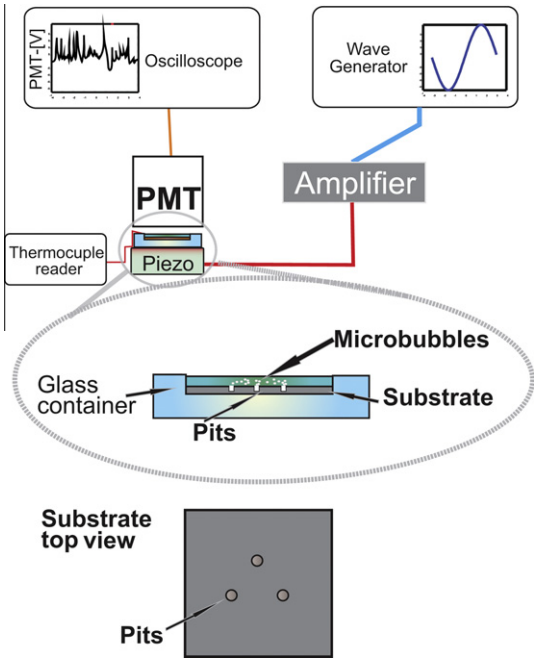

Fig. 1. Experimental setup (not to scale) showing the different components used. The zoomed inset shows the microreactor and a top view of a three-pit substrate.

The continuously applied acoustic field generated a standing wave depending on the height of the liquid column. For liquid heights close to one-quarter or three-quarters of the acoustic wavelength (approximately 250 or 300 μℓ volume of liquid, respectively) a pressure antinode is expected to be located on the substrate and a node at the free liquid–air interface. In this study frequencies of about 200 kHz with a corresponding water height of approximately 5 mm were used (250 μℓ).

A Hamamatsu E849-35 PMT (2.5 ns risetime), with 15 mm diameter glass window, amplified by a Canberra H.V. Supply Model 3002 was placed to capture the light emitted by the sonicated liquid on top of the chamber.

The experiments were conducted with different liquids but the same volumes (250 μℓ) at ambient conditions and open to the atmosphere. The voltage readout of the PMT corresponded to the SL and SCL emission, where applicable, from a certain population of bubbles.

The variations to the bottom surface (square silicon substrate of 10 mm width) of the micro-sonoreactor (the same as presented in [18]) were: blank with no pit (equivalent to a conventional US reactor of the bath type), one, two or three pits (small predefined cylindrical crevices on the silicon surface). The pits acted as nucleation sites for microbubble streamers that would otherwise not be present at the conditions studied. Details of the manufacturing process of the silicon substrate can be found in the Appendix sections.

Two different power settings were chosen out of the three presented in [18], corresponding to lower and higher power levels. The main reason to select these two settings is that they evidence a clear difference in the bubble pattern and the ultrasonic power being supplied to the whole system. Hence, we expect to see differences in the bubble populations capable of emitting light and producing radicals in all cases.

The controlled and localized acoustic microbubble generation can be sustained for at least several hours due to dissolved gas in the liquid transported into the pit by a process similar to rectified diffusion [4,41–43]. Since temperature and gas escaping the microchamber could not be controlled in this particular case, all experiments were carried out within 5–10 min.

For the SCL imaging, a digital SLR camera (Nikon D90) with 18–55 mm AFS zoom lens using the settings ISO1250, f 5.0 and a 60 s exposure time.

For SL imaging, a NF Multifunction synthesizer WF-1946A with a NF HSA-4014 amplifier, and a fan to cool the microreactor were used to get similar conditions as described before. The exposure time for experimental imaging and dark conditions subtraction was 10 min with a BitranBS-41L cooled CCD camera coupled to a Nikkor 35 mm lens and a magnifying glass.

3. Results and discussion

Contrary to the highly reproducible characteristics of single bubble cavitation, multiple bubbles are difficult to characterize since the bubble size distribution is constantly changing and bubbles do not cavitate always in phase with the driving frequency (period doubling and chaotic behaviors are reported elsewhere [44,45]). However, the overall multiple bubble activity can be quantified by measuring the total SL intensity. Fig. 2 shows PMT output recorded for 10 s for the three systems studied. Despite the appearance of emission spikes (common for these systems [21,46]), the average intensity of each system was used for comparison in the following discussion.

The emission spikes along a constant low intensity emission are short pulses that originate from specific bubbles that, upon reaching an appropriate size in the expansion phase, collapse and emit a strong light pulse. Micro-shocks occurring within the bubble during final collapse stages are reported elsewhere both for water and luminol solutions [47,46].

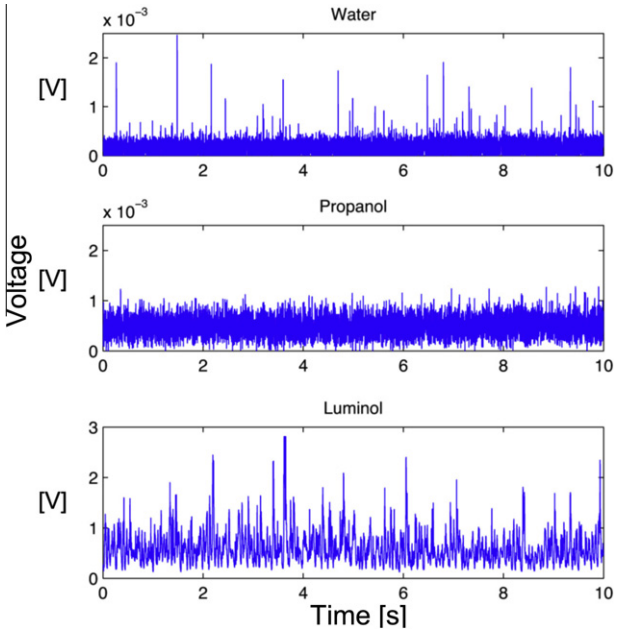

Fig. 2. Typical emission profiles recorded with the PMT for the different studied experimental conditions.

It can be seen in Fig. 2 that the emission spikes mainly appear for the water and luminol system and not that frequently for the aqueous propanol system. Despite the less frequent presence of these spikes in the propanol system, the average intensity was higher than that observed for water. This behavior provides evidence that the bubble population is largely transient as there is no SL quenching [48,39,49]. The presence of propanol can increase the bubble population by lowering the surface tension and facilitating the pinch-off events of microbubbles from the pit. The white space in between the signal and the "*x*-axis" for propanol and luminol, not present in plain water, is due to a higher overall SL and SCL intensity. A more detailed analysis for each system is presented in the following sections.

3.1. Water

When water is poured over the silicon substrate and US is switched on, a cloud of bubbles appears from the micropits at low power levels. An interesting behavior is observed when there are multiple pits driven at high power: the ejected bubbles travel to a common center point (see Fig. 3 and Supporting videos) due to a complex interplay of primary and secondary Bjerknes forces [18].

Fig. 4 shows a clear trend of increasing SL intensity with increasing number of pits, both at the low and high power regimes.

As the number of pits is increased, the number of SL active bubbles increases. The increase is almost double in the case of one-pit compared with the blank substrate. For two-pits, the SL enhancement is tripled, whilst for three-pits the SL is almost four times that of the blank substrate at high power. While a similar increase is observed at the higher power level, the relative increase with three-pits compared to two-pits is low. This might be due to stronger bubble clustering effects which are known to reduce the maximum expansion radius and shorten the bubble collapse duration [50].

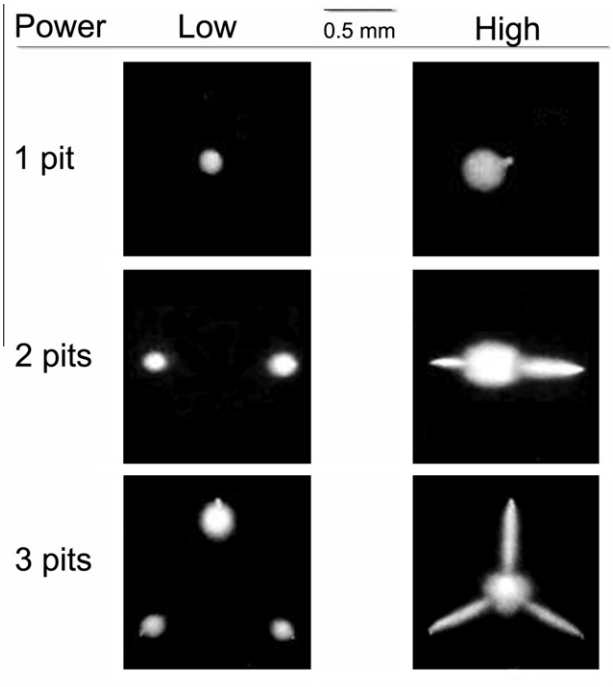

Fig. 3. Top view of the visible bubble streamers for the different scenarios studied. See Supporting videos.

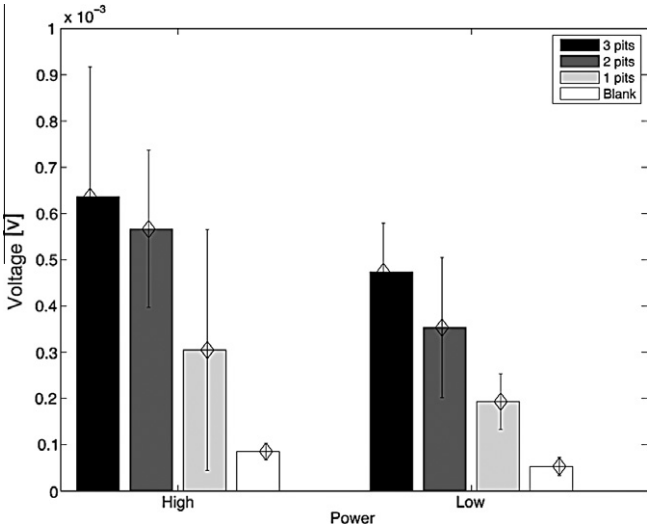

Fig. 4. Averaged SL intensities for the different studied experimental conditions in water.

When trying to image SL in the experiments with air-saturated Milli-Q water and the conditions described up to this point, not enough signal-to-noise images could be obtained. For this reason Milli-Q water was saturated with argon (Ar) and a glass slide was placed on top of the microreactor to avoid evaporation (see Supporting videos). During the imaging period the cooling of the piezo was carried out with a fan. The long exposure times required to obtain images like the ones presented in Fig. 5 made it very difficult to cover the same experimental conditions as for the rest of this work.

Nevertheless, these results allow us to conclude that the SL signal detected with the PMT was primarily due to light emission from the bubbles ejected from the micropits and not from random cavitation events in the bulk liquid.

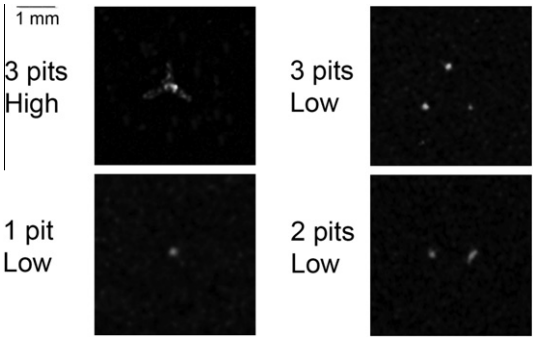

Fig. 5. SL image from bubble streamers for different scenarios. The top row corresponds to three-pit cases with similar pattern as observed under visible conditions for high and low power. The remaining figures correspond to one-, two-pit cases at low power.

3.2. Aqueous propanol solution

The visible bubble pattern for aqueous propanol solutions had no evident change when compared to water; however, as presented in Fig. 2, spikes present in the water emission profile are not as frequent in propanol solutions and the spike height is on average lower. The average intensities for propanol solutions are presented in Fig. 6.

Propanol can cause two effects in sonicated liquids: by adsorbing to the bubble solution interface it hinders bubble coalescence. And due to its volatile nature, it evaporates into the bubble and lowers the polytropic exponent, resulting in less heating inside the bubble [49]. These two effects can affect the SL in two ways. The hindrance to bubble coalescence has been shown to increase the number of transient cavitation bubbles [39]. The volatile nature leads to significant SL quenching in stable cavitation bubbles [51]. However, both processes need sufficient time for the propanol to accumulate at the bubble interface. Here, under the conditions of transient cavitation this time is not given. The observation that the average SL intensity for the propanol system instead of quenching the SL signal is higher than that observed in water is in agreement with the fact that the cavitation bubbles generated in the microreactor are transient in nature. As suggested earlier, the lower surface tension of the bubble stabilized on the pit due to the presence of propanol might yield a higher number of bubble streamers generated that in turn contribute to the increase in SL signal. This needs to be supported by future experiments with fast imaging of all these conditions.

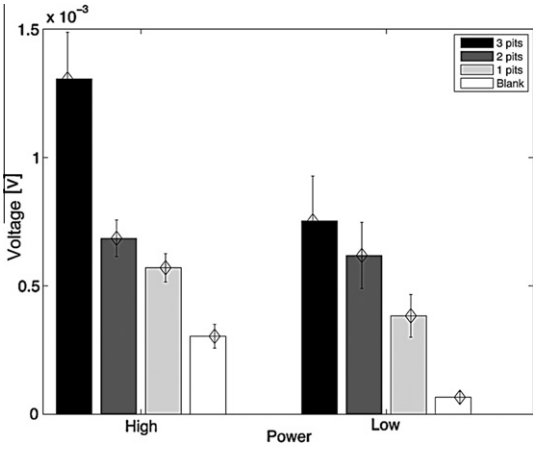

Fig. 6. Averaged SL intensities for the different studied experimental conditions with aqueous propanol solutions.

3.3. Luminol solution

Similar bubble streamer patterns from the luminol emission photographs are obtained (Fig. 7) to those observed in Fig. 3. The light emitted was bright enough to be seen with the naked eye in adjusted dark conditions.

As can be seen in these images, the SCL and hence radical formation is intensified at the location of the micropits. The average SCL intensities for the case of luminol solutions were several orders of magnitude higher than those from the SL in water as presented in Fig. 8. It is surprising then that the total emissions arising from the substrates containing pits are more or less identical to those arising from the blank substrate at low power. For the higher power, the two and three pits systems actually produce a lower yield than the blank substrate. It has been reported before that luminol SCL can have a unusual dependence with increasing power, sometimes reaching saturation and complete fading of intensity [46].

An explanation for our observations is that by driving the systems with two or more pits at high power, the shape of the bubbles in the cluster become deformed. This, combined with liquid flow inside the microreactor chamber, mixing, free liquid–air interface oscillation and temperature increase in less than 5 min can bring a change in the SCL.

We speculate that the observation of different SCL signal trends when compared to our previous study measuring OH· radicals [18] are due to the surface oscillation taking place at the liquid–air interface of the microreactor at the higher power conditions as reported before [52]. More details will be provided in the coming Section 3.4 and also in the Supplementary videos.

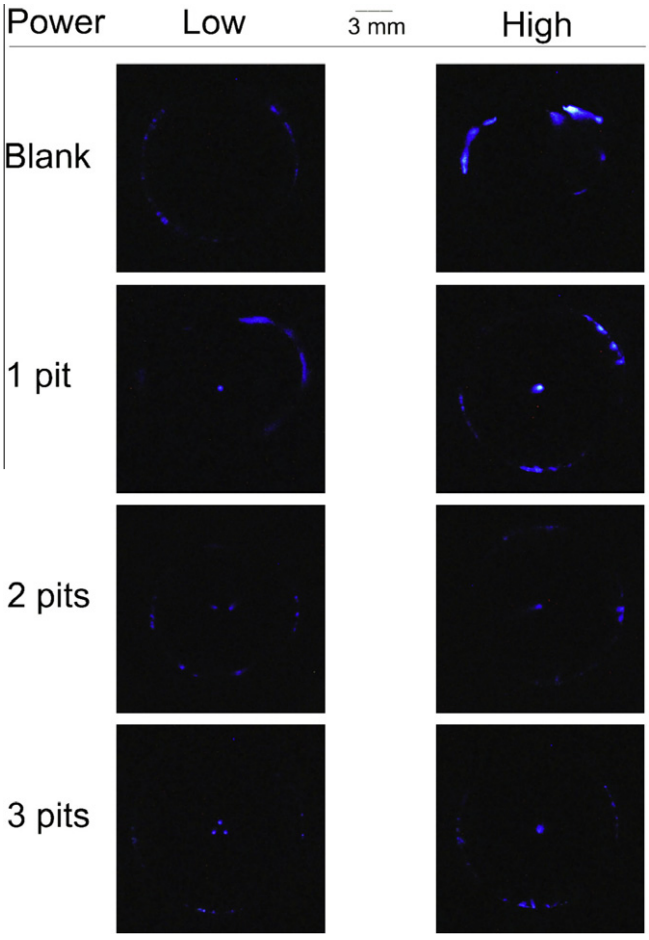

Fig. 7. Luminol solution images showing sonochemical active regions in white for the different scenarios studied.

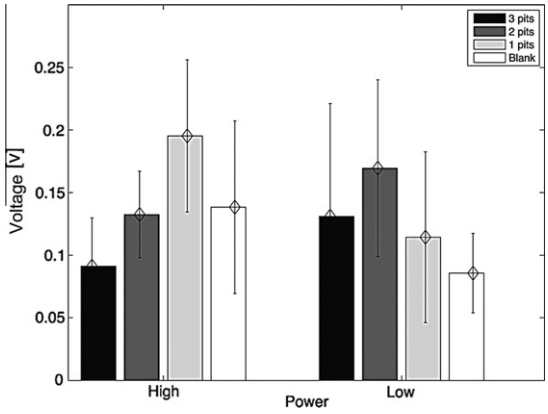

Fig. 8. Averaged SCL intensities for the different experimental conditions for aqueous luminol solution.

The pixel intensities of the luminol photographs were also averaged in time and are presented in Fig. 9. It can be seen that the two different experimental techniques (PMT and photographic imaging) produced similar trends (compare Fig. 8 and 9). From the photographic images taken, it can be seen that luminol emission is intensified not just at the location of the pits, but also at the edges of the substrate and other locations like cracks on the silicon substrate edge or the corners of the microchamber which can act as nucleation sites. Such effects occur across all the experiments and will be additive to the luminol emission from the pits. The PMT used to measure the SCL yield picks up light not just from the pits but also from the other places described.

3.4. Comparing SL and SCL

In Fig. 10 the relative increase of the SL intensity in water and propanol solutions is compared. Note that for all situations there is an increase in SL intensity of propanol over water as described before. For two- and one-pit cases the low power shows a higher relative value than at high power (when the bubble streamers tra-

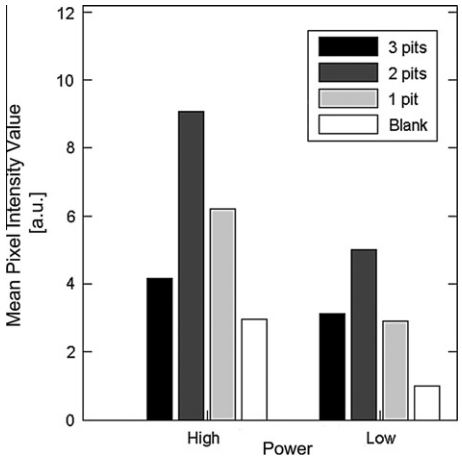

Fig. 9. Averaged pixel intensity values from the luminol images recorded (SCL) for the different experimental conditions for aqueous luminol solutions. Besides the blue light coming from the center of the silicon substrate (microbubbles generated from the pits) in some cases some SCL signal is seen coming from the edges of the substrate; presumably from crevices existing in the glass reaction chamber or substrate edges.

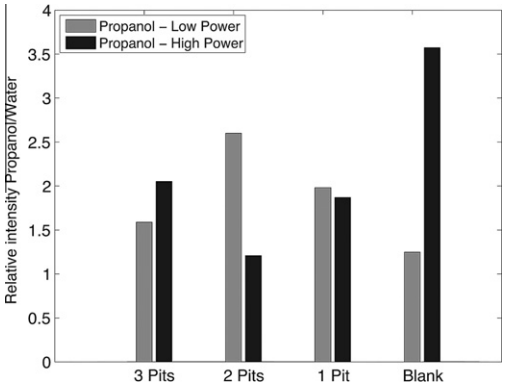

Fig. 10. Averaged SL intensities for the different experimental conditions for propanol solutions relative to water.

vel parallel to the wall and towards the center point) where the bubble population vary as the bubble clouds change their shape.

When comparing the relative increase in SCL intensity of luminol over the SL signal from water, Fig. 11 is obtained. Interestingly again the relative intensity is higher for the low power than for high power (now for the two- and three-pit systems) in line with our previous findings that higher power can be detrimental to $OH^{\cdot}$ radical formation [18]. This can be linked with the fact that at low power the population of smaller and more spherical bubbles is larger, and it is expected that these are the ones contributing the most to radical production. Another possibility according to numerical simulations is that $OH^{\cdot}$ production rate decreases at a too high temperature inside an air bubble as $OH^{\cdot}$ is consumed by oxidizing nitrogen inside a bubble [53]. This may suggest that on average, the temperature inside the bubbles is higher with pits compared to the blank conditions. Additionally, the bubble temperature is sometimes increased by the bubble–bubble interaction with smaller bubbles [54]. In the situation with pits, smaller and larger bubbles may result in higher bubble temperature inside larger bubbles compared to the case of no pit (blank) when there are mainly tiny bubbles (their size is too small to be recorded by the cameras).

Comparing Figs. 10 and 11 it can be seen that the blank case is a clear indication of the strong influence of the contribution from the bubbles generated at the pits. For the case of one pit it can be observed that there is almost no change in the relative intensity value for both the propanol and luminol when increasing power. This strongly evidences that the interaction of the microbubble streamers generated by more than one pit is an important factor in the trends observed (cluster–cluster interactions through shockwave emission).

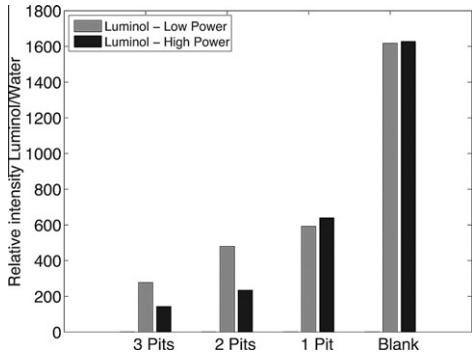

Fig. 11. Averaged SCL and SL intensities for the different experimental conditions for luminol solutions relative to water.

To partially illustrate the complexity of this system the influence of bubble–bubble and bubble–boundary interactions on the observed SL should be considered. When microbubbles are exposed to an acoustic field, if smaller than resonant size, they tend to travel to the pressure antinodes and cluster by virtue of Bjerknes forces. This behavior may influence the generated SL. An example is the case of high power for the two- and three-pit systems, where there is a change in the microbubble pattern when compared to the one-pit and blank configuration. A bubble cloud reflects and absorbs the sound field such that a lower intensity will be experienced by bubbles inside the cloud due to shielding. This reduces the intensity of the bubble collapse and the active bubble population, leading to a reduced SL intensity when compared to conventional multibubble cavitation [55]. As mentioned above bubble collapse in clusters also results in smaller expansion maximum radius and shorter collapse times [50].

It has been modeled and experimentally confirmed for a single bubble that the strength of the bubble collapse is affected by its translational movement (accelerated due to added mass forces while the driving pressure increases), and that the strength of the bubble collapse and its sphericity (i.e., the focusing power) are key ingredients determining the SL and SCL intensity [56–58,4]. Indeed, in our experiments higher SL is observed for higher power.

Referring back to Fig. 3: At high power, for the two- and three-pit cases (two last figures in the right column of Fig. 3), we see bubble clustering in between the pits, leading to a *depletion* of bubbles directly above the respective pits. Therefore, in these cases, the bubbles are actually only cavitating in a thin liquid layer of a width of about 200 μm above the surface [35]. Consequently, there is then less mutual shielding of the bubbles as compared to the other four cases (one-pit case at both powers and two- and three-pit cases at low powers). Additionally, at higher power there will be bubbles that expand to a larger size than at lower power, resulting in an increase in SL. We also expect that shockwave emissions from bubble clusters and cluster–cluster interactions (among microbubble streamers generated at each pit) influence the overall SL and SCL in terms of bubble maximum radius and collapse time as has been demonstrated before [50].

Observations at the highest power give evidence that water can occasionally splash out from the liquid–air interface due to acoustic radiation force (see Supplementary videos). This has been reported to decrease the efficiency of sonochemical reactions [52], consistent with the reduced SCL signal at high power and regimes with more than one pit. As the meniscus shakes vigorously (a sizzling sound accompanies this process), the cavitation field changes considerably in a way difficult to quantify or predict. This can introduce sources of errors in the SL and SCL measurements. In addition, at the highest power heating and degassing of the liquid occur faster and this obviously changes the conditions for SL and SCL.

It would be interesting to correlate the observed SL profile measured in this study to the influence of fluid mechanics such as flow due to acoustic streaming, microstreaming by meniscus oscillation, microbubbles flowing at different regimes, the interplay of secondary Bjerknes forces and bubble cluster interaction with the overall flow. Other factors such as closing the system with the presence of a glass slide on top of the microreactor to minimize liquid splashing, are among several other conditions that could be investigated but the appearance of degassing bubbles on the glass surface might be an undesired side-effect (see Supplementary videos). The above mentioned factors would influence the light emission, both from SL and SCL, at the different powers. As a last effort, continuous recording of these bubble streamers (in water, propanol and luminol solutions) may provide further clues to better understand our findings.

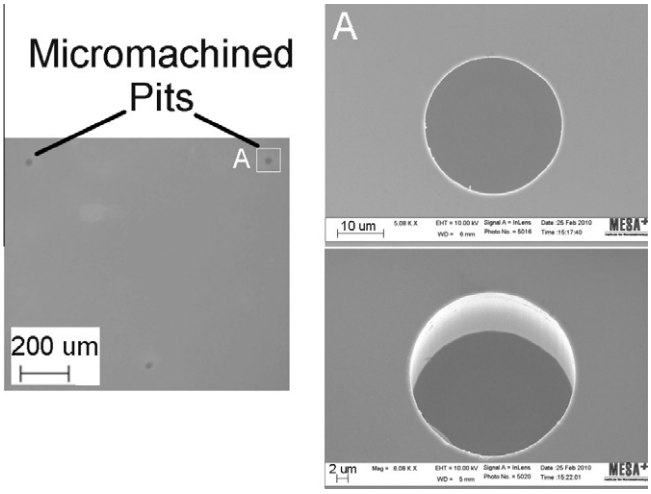

Fig. A.12. Pits etched on a silicone substrate. Top view, perspective view, top overview and distances.

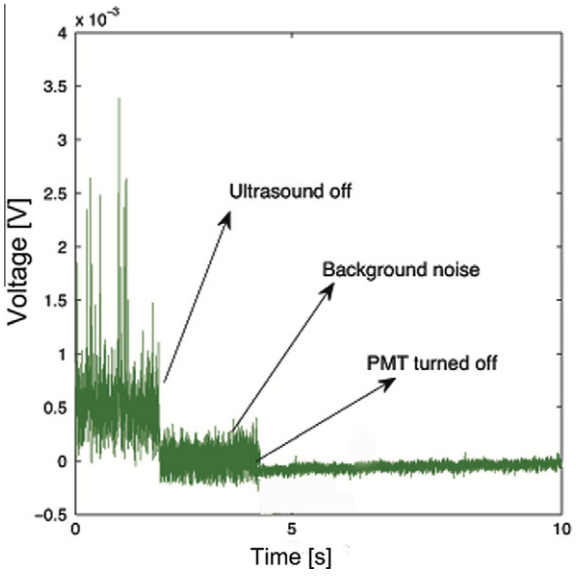

Fig. B.13. PMT read-out case in which given instants are pointed by arrows. The arrows mark the instant where the US signal and PMT amplifier are turned off.

4. Conclusions

We have measured light emission at a single frequency from different systems at two different power levels in the presence and absence of pits on surfaces. These pits promoted nucleation of microbubble streamers with distinctive streaming patterns at each power level. SL and SCL imaging provided evidence that the microbubbles arising from the pits are responsible for most of the light emission detected with PMT measurements. The presence of transient cavitation conditions was verified by measuring the SL intensity in propanol solutions. A difference in the light intensity of SL and SCL also led to the conclusion that there is a difference in the bubble population able to emit light and those which are chemically active. The multiple factors affecting the bubble streamers behavior are difficult to resolve individually. For that reason, there exists significant scope for future studies, particularly involving the control of the free surface liquid–air meniscus.

Acknowledgements

We thank Prof. Franz Grieser and Prof. Andrea Prosperetti for useful discussions and Stefan Schlautmann for technical assistance. This research was supported by the Technology Foundation STW, Applied Science Division of NWO and the Technology Programme of the Ministry of Economic Affairs, The Netherlands. The authors acknowledge financial support from the ARC, Australia.

Appendix A. Silicon substrate micromachining

Three different configurations of pits were designed. The pits had the same diameter (30 μm) and were arranged in sets of one, two (in a line) or three (in a triangle) at a distance of 1000 μm from each other (see Fig. A.12). The substrates were micromachined under clean room conditions on double-side polished silicon wafers and spin coated with the photosensitive substance Olin 12, on which the designed pattern was transferred with a mask aligner EV620 (photolitography). After development the pit pattern was open and with a plasma dry-etching machine Adixen AMS 100 SE (Alcatel) process BHARS, the holes were etched into the silicon substrate at the desired depth. The machined diced silicon square pieces of 1 cm-side were mounted to the bottom of a small glass container which contained a liquid volume of 250 μℓ, to the bottom of which a piezo element was attached.

Appendix B. PMT voltage levels

In Fig. B.13 the comparison of voltage read-out from the PMT when the ultrasound is turned off and when the PMT is turned off is shown.

Appendix C. Supplementary data

Supplementary data associated with this article can be found, in the online version, at http://dx.doi.org/10.1016/j.ultsonch.2012.04.008.

References

[1] M. Ashokkumar, J. Lee, S. Kentish, F. Grieser, Bubbles in an acoustic field: an overview, Ultrason. Sonochem. 14 (4) (2007) 470–475.
[2] D. Lohse, Sonoluminescence-Cavitation hots up, Nature 434 (2005) 33–34.
[3] Y.T. Didenko, K.S. Suslick, The energy efficiency of formation of photons radicals and ions during single-bubble cavitation, Nature 418 (6896) (2002) 394–397.
[4] M.P. Brenner, S. Hilgenfeldt, D. Lohse, Single bubble sonoluminescence, Rev. Mod. Phys. 74 (2002) 425–484.
[5] W. Lauterborn, T. Kurz, Physics of bubble oscillations, Rep. Prog. Phys. 73 (2010) 106501.
[6] M. Marinesco, J. Trillat, Action des ultrasons sur les plaques photographiques, Compt. Rend. 196 (1933) 858–860.
[7] H. Frenzel, H. Schultes, Luminescenz im ultraschallbeschickten wasser, Z. Phys. Chem. B27 (1934) 421.
[8] L. Crum, Sonoluminescence sonochemistry and sonophysics, J. Acoust. Soc. Am. 95 (1994) 559.
[9] E. Flint, K. Suslick, The temperature of cavitation, Science 253 (5026) (1991) 1397.
[10] T. Matula, R. Roy, Comparisons of sonoluminescence from single-bubbles and cavitation fields: bridging the gap, Ultrason. Sonochem. 4 (2) (1997) 61–64.
[11] W.B. McNamara III, Y. Didenko, K.S. Suslick, Effect of noble gases on sonoluminescence temperatures during multibubble cavitation, Phys. Rev. Lett. 84 (2000) 777–780.
[12] K. Suslick, Y. Didenko, M. Fang, T. Hyeon, K. Kolbeck, W. McNamara, M. Mdleleni, M. Wong, Acoustic cavitation and its chemical consequences, Philos. T. R. Soc. A 357 (1751) (1999) 335.
[13] K.S. Suslick, D.J. Flannigan, Inside a collapsing bubble: sonoluminescence and the conditions during cavitation, Annu. Rev. Phys. Chem. 59 (2008) 659–683.
[14] A. Brotchie, F. Grieser, M. Ashokkumar, Effect of power and frequency on bubble-size distributions in acoustic cavitation, Phys. Rev. Lett. 102 (8) (2009) 84302.

[15] K. Yasui, T. Tuziuti, J. Lee, T. Kozuka, A. Towata, Y. Iida, The range of ambient radius for an active bubble in sonoluminescence and sonochemical reactions, J. Chem. Phys. 128 (2008) 184705.
[16] D. Sunartio, K. Yasui, T. Tuziuti, T. Kozuka, Y. Iida, M. Ashokkumar, F. Grieser, Correlation between Na^* emission and Óchemically activeÒ acoustic cavitation bubbles, Chem Phys Chem 8 (16) (2007) 2331–2335.
[17] N.V. Dezhkunov, T.G. Leighton, Study into correlation between ultrasonic capillary effect and sonoluminescence, J. Eng. Phys. Thermophys. 77 (2004) 53–61.
[18] D. Fernandez Rivas, A. Prosperetti, A.G. Zijlstra, D. Lohse, H.J.G.E. Gardeniers, Efficient sonochemistry through microbubbles generated with micromachined surfaces, Angew. Chem. Int. Ed. 49 (50) (2010) 9699–9701.
[19] Y. Iida, K. Yasui, T. Tuziuti, M. Sivakumar, Y. Endo, Ultrasonic cavitation in microspace, Chem. Commun. (20) (2004) 2280–2281.
[20] J. Lee, T. Tuziuti, K. Yasui, S. Kentish, F. Grieser, M. Ashokkumar, Y. Iida, Influence of surface-active solutes on the coalescence clustering and fragmentation of acoustic bubbles confined in a microspace, J. Phys Chem. C 111 (51) (2007) 19015–19023.
[21] Tandiono, S. Ohl, D. Ow, E. Klaseboer, V. Wong, R. Dumke, C. Ohl, Sonochemistry and sonoluminescence in microfluidics, Proc. Natl. Acad. Sci. USA 108 (15) (2011) 5996–5998.
[22] N. Bremond, M. Arora, C.D. Ohl, D. Lohse, Controlled multi-bubble surface cavitation, Phys. Rev. Lett. 96 (2006) 224501.
[23] N. Bremond, M. Arora, S.M. Dammer, D. Lohse, Interaction of cavitation bubbles on a wall, Phys. Fluids 18 (12) (2006) 121505.
[24] P. Marmottant, J.P. Raven, H. Gardeniers, J.G. Bomer, S. Hilgenfeldt, Microfluidics with ultrasound-driven bubbles, J. Fluid Mech. 568 (2006) 109–118.
[25] B.M. Borkent, S. Gekle, A. Prosperetti, D. Lohse, Nucleation threshold and deactivation mechanisms of nanoscopic cavitation nuclei, Phys. Fluids 21 (10) (2009) 102003.
[26] G. Cravotto, P. Cintas, Harnessing mechanochemical effects with ultrasound-induced reactions, Chem. Sci. 2 (3) (2012) 295–307.
[27] A.J. Cobley, L. Edgar, M. Goosey, R. Kellner, T.J. Mason, Initial studies into the use of ultrasound to reduce process temperatures and chemical usage in the PCB desmear process, Circuit World 1 (37) (2011) 15–23.
[28] N.V. Dezhkunov, V. Dallacasa, Physical backgrounds for application of power ultrasound in fluorescent dye penetrant inspection. Proc. of 4th European Congress on Acoustics, Budapest, September 2005, pp. L231–L234.
[29] C.-D. Ohl, B. Wolfrum, Detachment and sonoporation of adherent HeLa-cells by shock wave-induced cavitation, BBA – Gen. Sub. 1624 (1–3) (2003) 131–138.
[30] R. Dijkink, S. Le Gac, E. Nijhuis, A. van den Berg, A. Vermes, A. Poot, C.-D. Ohl, Controlled cavitation-cell interaction: trans-membrane transport and viability studies, Phys. Med. Biol. 2 (53) (2008) 375.
[31] M. Ashokkumar, J. Lee, Y. Iida, K. Yasui, T. Kozuka, T. Tuziuti, A. Towata, Spatial distribution of acoustic cavitation bubbles at different ultrasound frequencies, ChemPhysChem 11 (8) (2010) 1680–1684.
[32] S. Hilgenfeldt, S. Grossmann, D. Lohse, A simple explanation of light emission in sonoluminescence, Nature 398 (6726) (1999) 402–405.
[33] S. Luther, R. Mettin, P. Koch, W. Lauterborn, Observation of acoustic cavitation bubbles at 2250 frames per second, Ultrason. Sonochem. 8 (3) (2001) 159–162.
[34] N. Tsochatzidis, P. Guiraud, A. Wilhelm, H. Delmas, Determination of velocity size and concentration of ultrasonic cavitation bubbles by the phase-doppler technique, Chem. Eng. Sci. 56 (5) (2001) 1831–1840.
[35] D. Fernandez Rivas, A.G. Zijlstra, L. Stricker, A. Prosperetti, D. Lohse, H.J.G.E. Gardeniers, Ultrasound nucleated microbubbles and their sonochemical radical production, Ultrason. Sonochem. ULTSON-D-12-00122 (in press).
[36] S. Labouret, J. Frohly, Bubble size distribution estimation via void rate dissipation in gas saturated liquid application to ultrasonic cavitation bubble fields, Eur. Phys. J. Appl. Phys. 19 (01) (2002) 39–54.
[37] W. Chen, T. Matula, L. Crum, The disappearance of ultrasound contrast bubbles: observations of bubble dissolution and cavitation nucleation, Ultrasound Med. Biol. 28 (6) (2002) 793–803.
[38] M. Ashokkumar, J. Lee, Y. Iida, K. Yasui, T. Kozuka, T. Tuziuti, A. Towata, The detection and control of stable and transient acoustic cavitation bubbles, Phys. Chem. Chem. Phys. 11 (43) (2009) 10118–10121.
[39] G. Price, M. Ashokkumar, F. Grieser, Sonoluminescence quenching of organic compounds in aqueous solution: frequency effects and implications for sonochemistry, J. Am. Chem. Soc. 126 (9) (2004) 2755–2762.
[40] R. Toegel, B. Gompf, R. Pecha, D. Lohse, Does water vapor prevent upscaling sonoluminescence?, Phys Rev. Lett. 85 (15) (2000) 3165–3168.
[41] R.E. Apfel, The role of impurities in cavitation-threshold determination, J. Acoust. Soc. Am. 48 (5B) (1970) 1179–1186.
[42] L. Crum, Nucleation and stabilization of microbubbles in liquids, Appl. Sci. Res. 38 (1) (1982) 101–115.
[43] J.B. Fowlkes, L.A. Crum, Cavitation threshold measurements for microsecond length pulses of ultrasound, J. Acoust. Soc. Am. 83 (6) (1988) 2190–2201.
[44] W. Lauterborn, E. Cramer, Subharmonic route to chaos observed in acoustics, Phys. Rev. Lett. 47 (20) (1981) 1445–1448.
[45] C. Cabeza, A. Sicardi-Schifino, C. Negreira, G. Montaldo, Experimental detection of a subharmonic route to chaos in acoustic cavitation through the tuning of a piezoelectric cavity, J. Acoust. Soc. Am. 103 (1998) 3227.
[46] K. Negishi, Experimental studies on sonoluminescence and ultrasonic cavitation, J. Phys. Soc. Jpn. 16 (7) (1961) 1450–1465.
[47] P. Jarman, Sonoluminescence: a discussion, J. Acoust. Soc. Am. 32 (1960) 1459.
[48] J. Lee, S. Kentish, M. Ashokkumar, The effect of surface-active solutes on bubble coalescence in the presence of ultrasound, J. Phys. Chem. B 109 (11) (2005) 5095–5099.
[49] R. Toegel, S. Hilgenfeldt, D. Lohse, Suppressing dissociation in sonoluminescing bubbles: the effect of excluded volume, Phys. Rev. Lett. 88 (2002) 034301.
[50] K. Yasui, Y. Iida, T. Tuziuti, T. Kozuka, A. Towata, Strongly interacting bubbles under an ultrasonic horn, Phys. Rev. E 77 (1) (2008) 016609.
[51] J. Guan, T. Matula, Time scales for quenching single-bubble sonoluminescence in the presence of alcohols, J. Phys. Chem. B 107 (34) (2003) 8917–8921.
[52] T. Tuziuti, K. Yasui, T. Kozuka, A. Towata, Influence of liquid-surface vibration on sonochemiluminescence intensity, J. Phys. Chem. A 114 (27) (2010) 7321–7325.
[53] K. Yasui, T. Tuziuti, Y. Iida, Optimum bubble temperature for the sonochemical production of oxidants, Ultrasonics 42 (1) (2004) 579–584.
[54] K. Yasui, A. Towata, T. Tuziuti, T. Kozuka, K. Kato, Effect of static pressure on acoustic energy radiated by cavitation bubbles in viscous liquids under ultrasound, J. Acoust. Soc. Am. 130 (5) (2011) 3233–3242.
[55] Z. Zeravcic, D. Lohse, W. van Saarloos, Collective oscillations in bubble clouds, J. Fluid Mech. 680 (2011) 114–149.
[56] M.P. Brenner, D. Lohse, T.F. Dupont, Bubble shape oscillations and the onset of sonoluminescence, Phys. Rev. Lett. 75 (1995) 954–957.
[57] R. Sadighi-Bonabi, R. Rezaei-Nasirabad, Z. Galavani, The dependence of the moving sonoluminescing bubble trajectory on the driving pressure, J. Acoust. Soc. Am. 126 (2009) 2266.
[58] S. Hatanaka, H. Mitome, K. Yasui, S. Hayashi, Single-bubble sonochemiluminescence in aqueous luminol solutions, J. Am. Chem. Soc. 124 (35) (2002) 10250–10251.